

Reconstruction of Orion EDU Parachute Inflation Loads

Eric S. Ray¹

Jacobs Engineering, Houston, TX, 77058

The process of reconstructing inflation loads of Capsule Parachute Assembly System (CPAS) has been updated as the program transitioned to testing Engineering Development Unit (EDU) hardware. The equations used to reduce the test data have been re-derived based on the same physical assumptions made by simulations. Due to instrumentation challenges, individual parachute loads are determined from complementary accelerometer and load cell measurements. Cluster inflations are now simulated by modeling each parachute individually to better represent different inflation times and non-synchronous disreefing. The reconstruction procedure is tailored to either infinite mass or finite mass events based on measurable characteristics from the test data. Inflation parameters are determined from an automated optimization routine to reduce subjectivity. Infinite mass inflation parameters have been re-defined to avoid unrealistic interactions in Monte Carlo simulations. Sample cases demonstrate how best-fit inflation parameters are used to generate simulated drag areas and loads which favorably agree with test data.

Nomenclature

BEA	=	Best Estimate Atmosphere
BET	=	Best Estimate Trajectory
BEW	=	Best Estimate Winds
C_D	=	Drag coefficient
C_{D_o}	=	Drag coefficient related to full open canopy, normalized to total system weight and rate of descent
$(C_{D_S})(t)$	=	Drag area growth as a function of time
$(C_{D_S})_o$	=	Full open drag area
$(C_{D_S})_{p,i}$	=	Dynamic drag area of individual parachute i
$(C_{D_S})_v$	=	Effective drag area of payload or test vehicle
CDT	=	Cluster Development Test (series)
CM	=	Crew Module
CPAS	=	Capsule Parachute Assembly System
Δ , delta	=	Uncertainty in a measurement or calculated value
DGPS	=	Differential Global Positioning System
D_o	=	Nominal parachute diameter based on reference area, $D_o = \sqrt{4 \cdot S_o / \pi}$
DSS	=	Decelerator System Simulation
EDU	=	Engineering Development Unit
ε_{i-1}	=	Reefing area ratio at end of previous stage
ε_i	=	Reefing area ratio at the end of stage i, $\varepsilon_i = (C_{D_S})_R / (C_{D_S})_o$
expopen	=	Opening profile shape exponent: < 1 concave down; = 1 linear; > 1 concave up
F_i	=	Tension force in a parachute riser
g	=	Acceleration of Earth Gravity
γ	=	Flight path angle
Gen	=	Generation
GPS	=	Global Positioning System
IMU	=	Inertial Measurement Unit
m_p	=	Mass of parachute and suspension equipment
MPCV	=	Multi Purpose Crew Vehicle (Orion)

¹ Analysis Engineer, Aeroscience and Flight Dynamics, 2224 Bay Area Blvd, Houston, TX, AIAA Member.

m_v	=	Mass of test vehicle, not including canopies and suspension equipment
n	=	Canopy fill distance, normalized to reference diameter
N_c	=	Number of parachutes in a cluster
n_p	=	Distance (measured in reference diameters) to peak drag area (infinite mass only)
\bar{q} , q_{bar}	=	Dynamic pressure, $\bar{q} = \frac{1}{2} \cdot \rho \cdot V_{air}^2$
RAWIN	=	Radar Wind Sounding (weather balloon)
ρ , rho	=	Humidity-corrected atmospheric density
RC	=	Ramp Clear (usually chosen as start of test)
RSS	=	Root-Sum-of-Squares
σ , sigma	=	Standard deviation (general)
S_o	=	Parachute canopy full open reference area based on constructed shape including vents and slots
SPAN	=	Synchronized Position Attitude & Navigation
t_f	=	Canopy fill time from either bag strip or disreef to completion of stage inflation
t_{fp}	=	Time from either bag strip or disreef to occurrence of peak drag area
t_i	=	Inflation start time of either bag strip or the disreef event from a previous stage
θ_i , theta	=	Fly-out angle for parachute i
t_k	=	Time to ramp down after stage over-inflation
TSPI	=	Time Space Position Information
V_{air}	=	Total airspeed relative to air mass
V_e	=	Equilibrium rate of descent
V_{e_o}	=	Sea level equivalent rate of descent
V_i	=	Velocity (airspeed) at beginning of each stage at time t_i
$W_{p,i}$	=	Dry weight parachute i
W_T	=	Total weight of test vehicle, deployed parachutes, and suspension equipment
W_v	=	Suspended weight of test vehicle, not including canopies and suspension equipment

I. Introduction

FLIGHT tests of the Capsule Parachute Assembly System (CPAS) achieve two main purposes. First, successful deployments of representative Orion/Multi Purpose Crew Vehicle (MPCV) hardware under realistic conditions provide confidence in the design. Second, the test data collected are used to develop parameters for high-fidelity Monte Carlo simulations.¹ Simulations will always outnumber the budgeted number of flight tests that can be executed, and these simulations may be run under conditions not achievable by the available test vehicles.²

CPAS simulation tools have evolved over the course of the test program from simple spreadsheets to high-fidelity 6-DOF multi-body applications. The types and amount of measured flight test data have also increased considerably. A flow diagram of the typical test data reconstruction process is shown in Figure 1. Information is first assembled into “Best Estimate” Atmosphere, Wind, and Trajectory files. The equations used to compute the atmospheric properties and uncertainties from sensor data were previously published in Ref. 3. That publication also contains an in-depth explanation of how trajectory data are obtained from optical Time Space Position Information (TSPI), Differential Global Positioning Systems (DGPS), and an Inertial Measurement Unit (IMU) coupled with GPS. Uncertainties are also propagated with the measured quantities to estimate uncertainties in final data products.

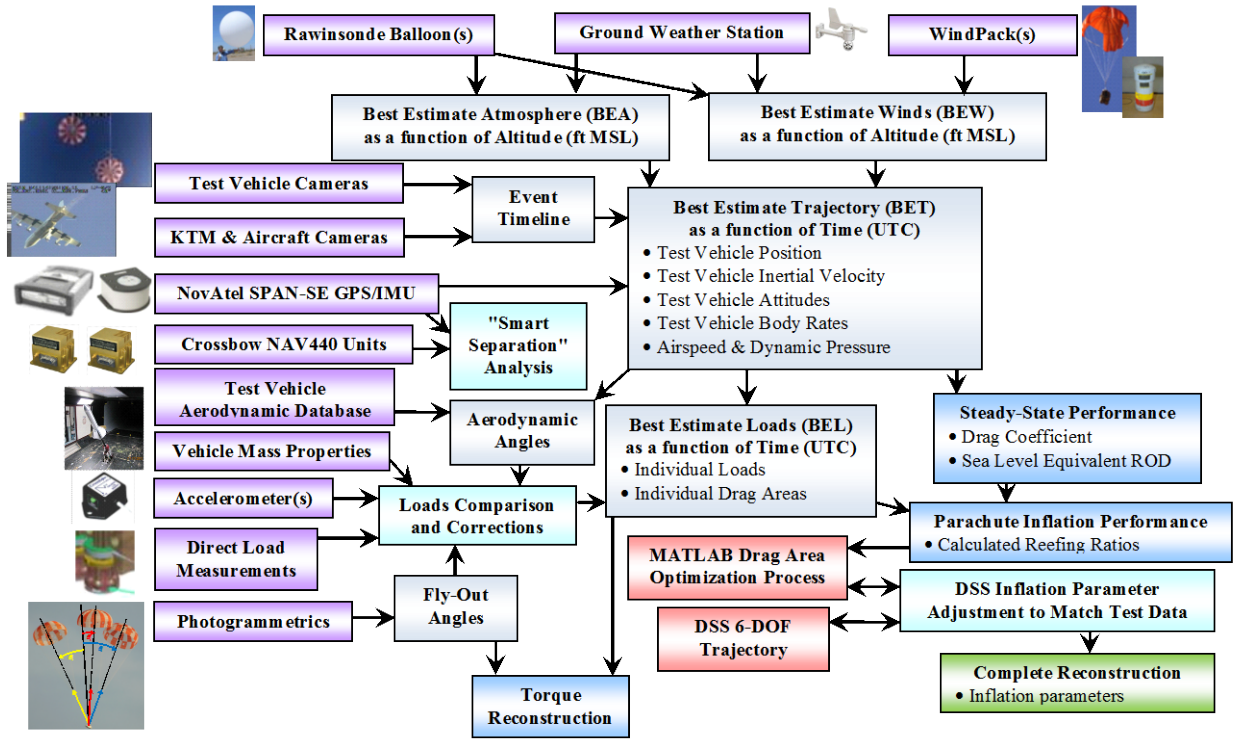


Figure 1. Overall test data reconstruction process.

This paper will build on previous CPAS publications by outlining the parachute data reduction process for loads performance. CPAS analysis capabilities are currently evolving from simulating total cluster loads as a “composite parachute” towards modeling each parachute individually, a change that is expected to eliminate over-conservatism in predicted loads due to the elimination of unrealistic load-sharing assumptions. To this end, parachute inflation loads are determined via accelerometers and direct tension measurements, from which parachute drag areas are calculated. This paper will also describe how the drag area growth curves are reconstructed to determine the inflation parameters that best match the actual inflations while keeping the simulated trajectory (position, velocity, etc.) as close to the test data as possible.

II. Equations and Assumptions

A comprehensive derivation of the parachute system was conducted in order to ensure that test data are correctly compared to simulations. Figure 2 shows a simplified free-body diagram of the forces involved in unsteady parachute deceleration. Postflight analysis of the test data currently neglects the enclosed and apparent mass (collectively referred to as “added mass”) because they are not measured directly.⁴ Added mass and riser spring effects are accounted for later in the simulation codes. While the riser tension force can be directly measured, the total force on the inflating parachute cannot, and is computed from other measured quantities.

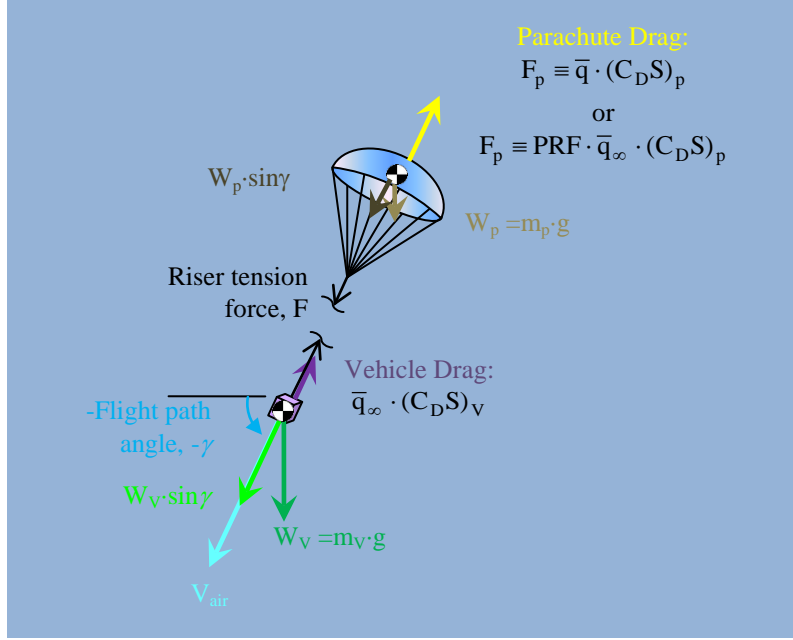


Figure 2. Simplified free-body diagram of a decelerating parachute system.

When a vehicle generates a significant wake, its parachute will experience a dynamic pressure, \bar{q} , that is some fraction of the freestream dynamic pressure, \bar{q}_∞ , measured at the forebody. The ratio of parachute local dynamic pressure to freestream dynamic pressure is defined as the Pressure Recovery Fraction (PRF).

The free-body diagram is used to generate two equations depending on where its boundary is drawn. For Eq. 1 it encompasses the entire system. For Eq. 2 it only includes the test vehicle. The forces are assumed to act along the airspeed direction which is also assumed to be the direction of deceleration.

$$\text{PRF} \cdot \bar{q}_\infty \cdot (C_D S)_p + \bar{q}_\infty \cdot (C_D S)_v - W_v \cdot \sin \gamma - W_p \cdot \sin \gamma = m_p \cdot a_p + m_v \cdot a_v \quad (1)$$

$$F + \bar{q}_\infty \cdot (C_D S)_v - W_v \cdot \sin \gamma = m_v \cdot a_v \quad (2)$$

To solve these equations for acceleration (assumed to be the same for the parachute and vehicle), mass and gravity product terms are substituted for vehicle weight, W_v , and parachute weight, W_p . Both equations are solved for acceleration to form Eq. 3 and Eq. 4, respectively.

$$\frac{\bar{q}_\infty \cdot (\text{PRF} \cdot (C_D S)_p + (C_D S)_v)}{(m_v + m_p)} = (a_v + g \cdot \sin \gamma) \quad (3)$$

$$\frac{F + \bar{q}_\infty \cdot (C_D S)_v}{m_v} = (a_v + g \cdot \sin \gamma) \quad (4)$$

A. Load and Dynamic Drag Area from Sensed Acceleration

Accelerometers on the test vehicle will detect a “sensed acceleration” that includes gravity, g . For example, at rest the readings are $[0.0, 0.0, 1.0] \cdot g$. The load factor, G , is defined in terms of the sensed acceleration in Eq. 5.

$$\frac{\bar{G}}{g} = (\bar{a}_v + \bar{g}) \quad (5)$$

Assuming all deceleration acts along the velocity direction, the magnitude of the sensed acceleration in that direction is equal to the right hand side expressions of Eq. 3 and Eq. 4. The sensed load factor is then substituted into

Eq. 4 to solve for riser load in Eq. 6. This equation is very useful for estimating the total parachute loads on the test vehicle when no direct load measurements are possible. It is also used to help calibrate direct load measurements.

$$F = m_v \cdot \left(\frac{G}{g} \right) - \bar{q}_\infty \cdot (C_D S)_v \quad \text{or} \quad F = W_v \cdot G - \bar{q}_\infty \cdot (C_D S)_v \quad (6)$$

The uncertainty of computed data are determined according to the partial fraction and Root-Sum-of-Squares (RSS) methods from Ref. 5. This assumes that the input data errors are uncorrelated. Applying this method to Eq. 6 provides the uncertainty in the load computation, $|\Delta F|$, as shown in Eq. 7.

$$|\Delta F| = \left[\left(|\Delta W_v| \cdot G \right)^2 + \left(|\Delta G| \cdot W_v \right)^2 + \left(|\Delta \bar{q}_\infty| \cdot (C_D S)_v \right)^2 + \left(|\Delta (C_D S)_v| \cdot \bar{q}_\infty \right)^2 \right]^{1/2} \quad (7)$$

Similarly, the parachute dynamic drag area, $(C_D S)_p$, in terms of acceleration can be determined by substituting the sensed load factor into Eq. 3. The result is presented as Eq. 8 where W_T is the total weight of the vehicle and deployed parachute.

$$\text{PRF} \cdot (C_D S)_p = \frac{m_v + m_p}{\bar{q}_\infty} \cdot \left(\frac{G}{g} \right) - (C_D S)_v \quad \text{or} \quad \text{PRF} \cdot (C_D S)_p = \frac{W_T \cdot G}{\bar{q}_\infty} - (C_D S)_v \quad (8)$$

The uncertainty in the dynamic drag area from accelerometers is computed in Eq. 9.

$$|\Delta \text{PRF} \cdot (C_D S)_p| = \left[\left(\frac{|\Delta W_T| \cdot G}{\bar{q}_\infty} \right)^2 + \left(\frac{|\Delta G| \cdot W_T}{\bar{q}_\infty} \right)^2 + \left(\frac{|\Delta \bar{q}_\infty| \cdot W_T \cdot G}{\bar{q}_\infty^2} \right)^2 + \left(|\Delta (C_D S)_v| \right)^2 \right]^{1/2} \quad (9)$$

Although Eq. 6 and Eq. 8 were derived from a system with one parachute, they can also be applied to a cluster of parachutes by assuming the sum of the parachute masses is m_p and $(C_D S)_p$ is the total drag area of the cluster.

B. Dynamic Drag Area from Riser Tension

In order to obtain the drag area of a single inflating parachute in a cluster, one can construct a free-body diagram of only the parachute from Figure 2. The riser tension of a single parachute is defined as F_i , the parachute mass as $m_{p,i}$, and the individual drag area as $(C_D S)_{p,i}$. The forces and accelerations are listed in Eq. 10.

$$-F_i + \text{PRF} \cdot \bar{q}_\infty \cdot (C_D S)_{p,i} - W_{p,i} \cdot \sin \gamma = m_p \cdot a_p \quad (10)$$

Convert the weights to m-g and assume the vehicle accelerometer reading also applies to the parachute as before. Substituting the sensed load factor, the drag area is solved for in Eq. 11.

$$\text{PRF} \cdot (C_D S)_{p,i} = \frac{F_i + m_{p,i} \cdot \left(\frac{G}{g} \right)}{\bar{q}_\infty} \quad \text{or} \quad \text{PRF} \cdot (C_D S)_{p,i} = \frac{F_i + W_{p,i} \cdot G}{\bar{q}_\infty} \quad (11)$$

Note that a correction from the accelerometer reading (G) should be used in conjunction with the riser load reading (F_i) in order to evaluate the dynamic drag area of the parachute. Postflight data reconstructions from previous generations of CPAS flight tests neglected this acceleration term. Although neglecting this term would be a valid assumption if the dry mass of parachute is much less than the mass of the test vehicle, it is not a good assumption for the CPAS Main parachutes where the parachute weight is a large fraction of the total weight (~1,000 lbm / 20,000 lbm = 5%).

The uncertainty of dynamic drag area is determined according to Eq. 12.

$$|\Delta(C_{DS})_{p,i}| = \left[\left(\frac{|\Delta F_i|}{\bar{q}_\infty} \right)^2 + \left(\frac{|\Delta W_{p,i}| \cdot G}{\bar{q}_\infty} \right)^2 + \left(|\Delta G| \cdot \frac{|\Delta G| \cdot W_{p,i}}{\bar{q}_\infty} \right)^2 + \left(|\Delta \bar{q}_\infty| \cdot \frac{F_i + W_{p,i} \cdot G}{\bar{q}_\infty^2} \right)^2 \right]^{1/2} \quad (12)$$

III. Parachute Load Measurements for CPAS EDU Tests

As the CPAS test vehicles have become more representative of the Orion vehicle hardware, measuring riser tension has become more challenging. Two redundant methods of determining parachute loads and drag areas are used to complement each other.

A. Load Measurement Instrumentation

The first method to compute the total loads is using the accelerometer readings with the previously derived equations. Generally, the accelerometer housed in the IMU⁶ of a NovAtel SPAN-SE (Synchronized Position Attitude & Navigation)⁷ is used.

The second method is to measure individual riser tension. Previous generations of flight test vehicles installed strain links in the load path above a confluence fitting and below textile risers. These strain links could no longer be used with the current CPAS design of steel risers attaching to the structure at a single-point attachment.

Custom Futek load cells are now attached to ends of the Drogue and Main steel riser in the “flowerpot” to measure individual parachute loads. These measure the compression force as the steel riser tension pulls the “puck” terminations towards the bottom of the flowerpot. This is illustrated in Figure 3.

The load cells have several advantages over the accelerometers for measuring loads. Load cells can measure individual parachute loads but accelerometers only measure the total load. Isolating the total parachute load with accelerometers requires estimating the forebody aerodynamic drag of the test vehicle. Finally, the accelerometers will produce much more noise than the load cells during dynamic events such as mortar deployment.

However, the load cells have one significant drawback. Because they are located within the vehicle structure, the true parachute loads will be higher than the readings because some tension force is lost through friction between the steel risers bending over the fairlead and risers rubbing and twisting against each other. The “friction losses” are noticeably large when the test vehicle is unstable and parachute fly-out angles are large. The Drogue and Main parachute load paths are illustrated in Figure 4.

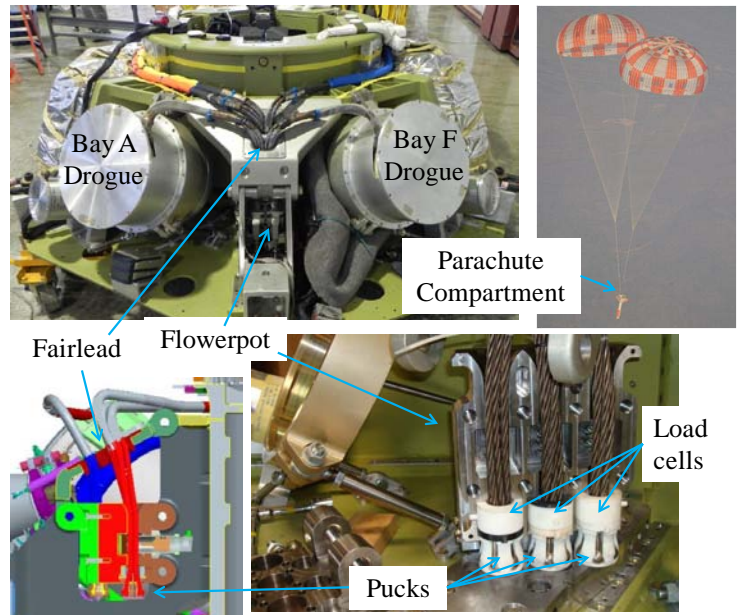


Figure 3. Load cell installation within parachute compartment.

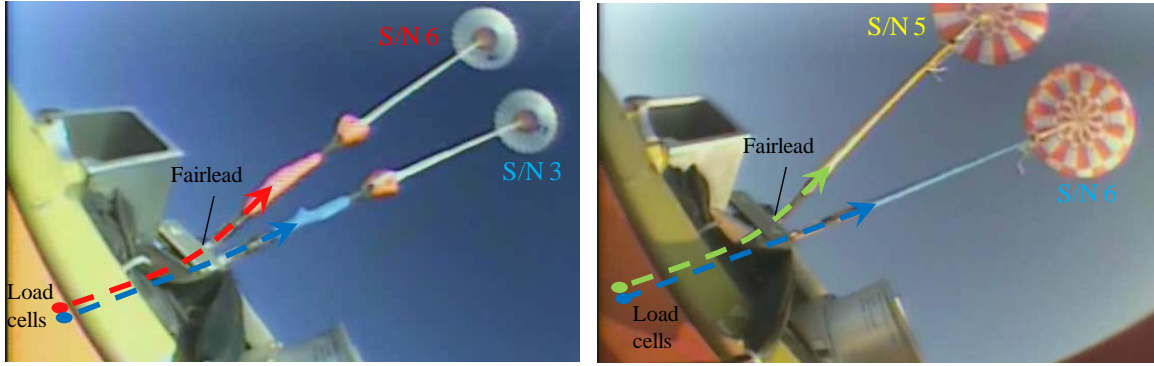


Figure 4. Load path of EDU Drogue parachutes (left) and EDU Main parachutes (right).

A method of compensating for the friction losses in the load cells was developed by using the accelerometer data. First, the total parachute drag area is computed for each stage using accelerometer data via Eq. 8. Next, individual parachute drag areas are computed from load cell data using Eq. 11. The sum of the load cell drag area should be equal to the accelerometer drag area for each stage after the inflation transients have occurred. The load cell data are scaled based on accelerometer drag areas.

B. Drogue Parachute Example

An example of this process from the Drogue phase of Cluster Development Test (CDT)-3-2 is shown in Figure 5. This test had a reefed phase leading into a full open Drogue phase. The mean steady-state drag areas for each phase were computed using the IMU accelerometer as 238.6 and 501.5 ft². The sum of the load cell data were time averaged during these same durations. Scale factors of 1.159 and 1.107 were computed between the lower and higher readings at the midpoints of each phase. It is likely that the scale factor is lessened as the Drogue becomes more stable and the steel risers are bent less severely over the fairlead. Therefore, a linear trend was drawn between these two points to vary the load cell data scale factor vs. time.

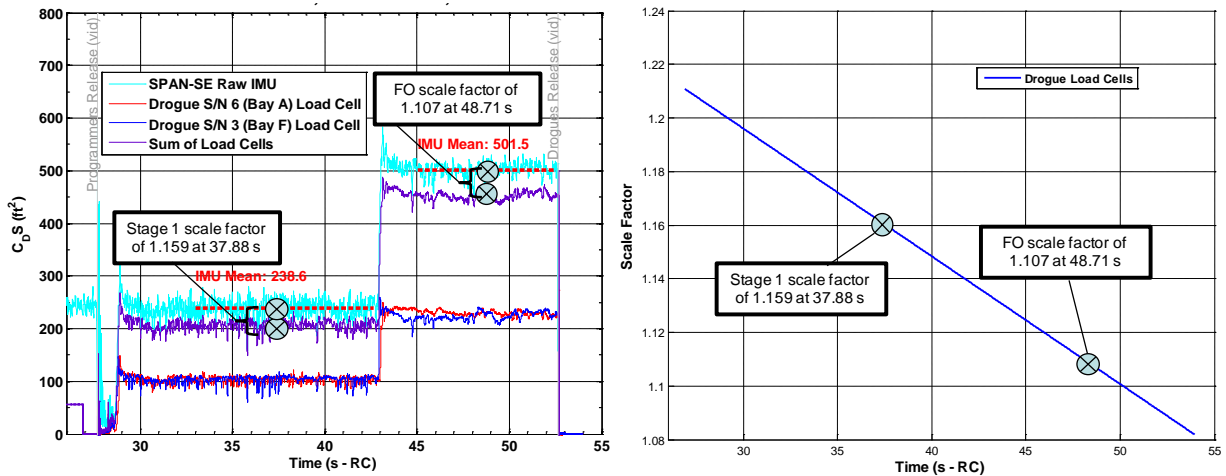


Figure 5. CDT-3-2 EDU Drogue accelerometer and load cell drag areas (left) and varying scale factor (right).

This varying scale factor is applied to each Drogue load cell reading and the load cell drag area is re-computed. The results are shown in Figure 6. As expected, the sum of the load cell data generally matches the accelerometer data. The accelerometers have slightly more noise.

After scaling, the total Drogue load cell peak load for the first stage was 28,270 lbf, which is about equal to the peak load from the IMU accelerometer of 28,330 lbf.

Another metric which can be obtained from cluster loads is the relative load share. Load share can be computed at several instants: when the global peak (sum of both Drogue loads) occurred, when the S/N 6 peak occurred, when the S/N 3 peak occurred, and using a time independent method. In this case, the average first stage load share from all four methods was 58/42. The preflight predictions used a worst case load share of 65/35 based on Apollo experience.

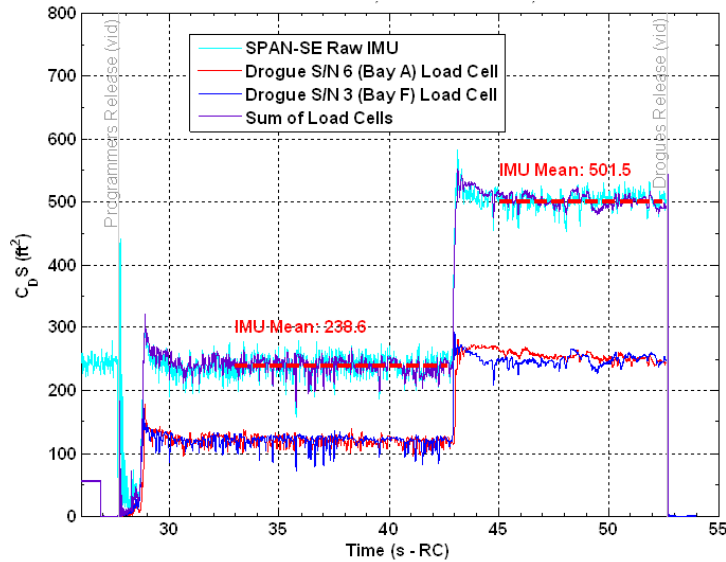


Figure 6. Scaled load cell drag area compared with accelerometer drag area.

C. Main Parachute Example

The mean dynamic drag areas from the load cells were compared with the mean drag areas from the accelerometers at the first and second stage, as shown in Figure 7 and Figure 8. Because the scale factor for both stages was the same, a constant scale factor was applied to all the Main load cell data. The scaling factor forces the mean load cell drag area (purple) to match the IMU-derived drag area (cyan).

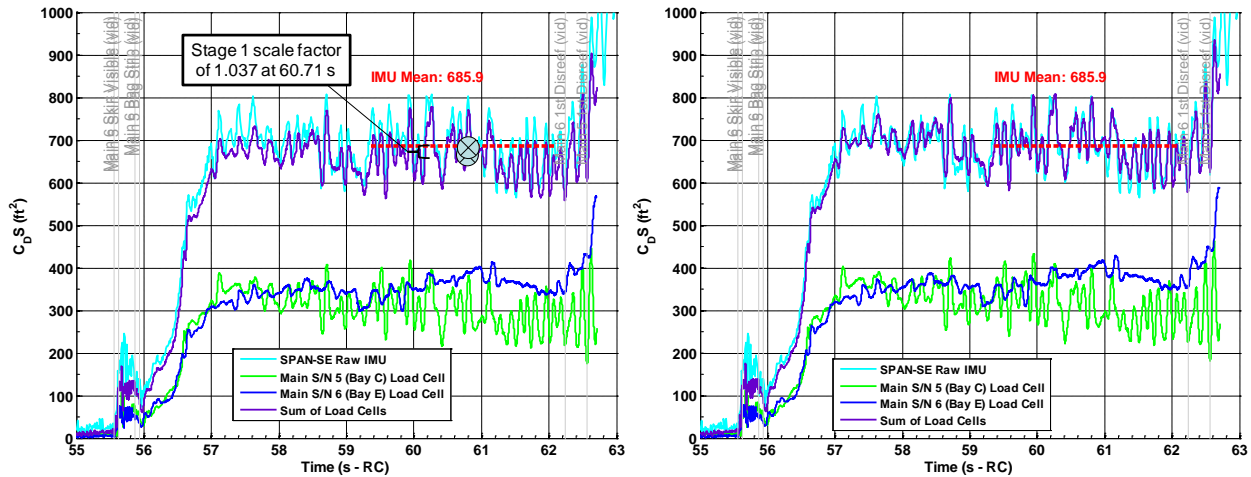


Figure 7. CDT-3-2 EDU Main 1st stage load cell data before (left) and after scaling (right) to match accelerometer data.

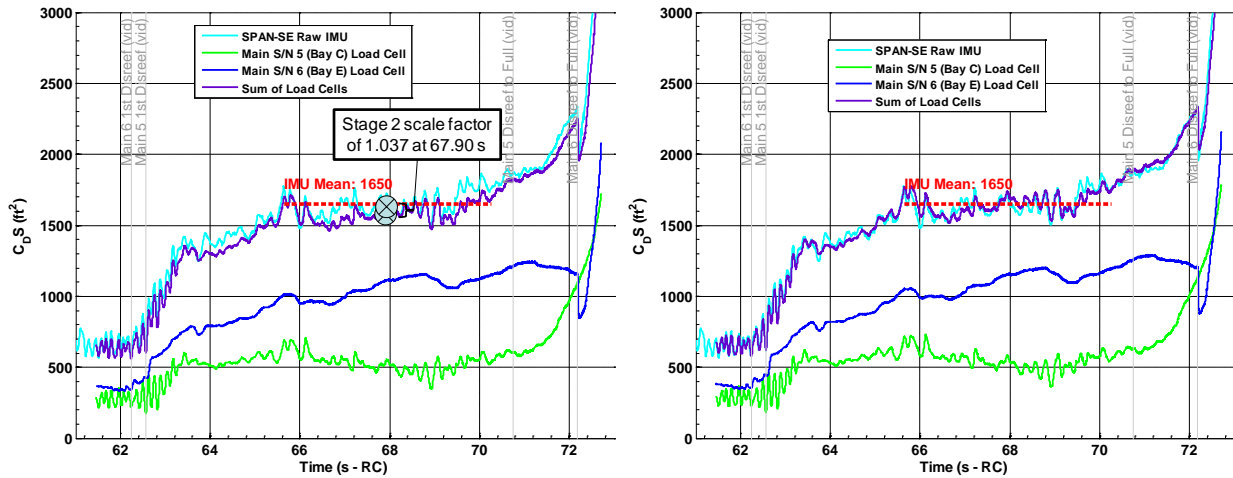


Figure 8. CDT-3-2 EDU Main 2nd stage load cell data before (left) and after scaling (right) to match accelerometer data.

D. Fly-Out Angle Correction

Another correction applied to the Main data is to account for the fly-out angles. The fly-out angle photogrammetric method and results are discussed in Ref. 8 and updates to the method are in Ref. 9. As illustrated in Figure 9 (left), the sum of the magnitude of the load cells will exceed the computed load from the accelerometers, which is along the axis of deceleration. The corrected load (right) is computed as the sum of the products of each parachute's load cell tension reading, F_i , and the cosine of its fly-out angle, θ_i , according to Eq. 13.

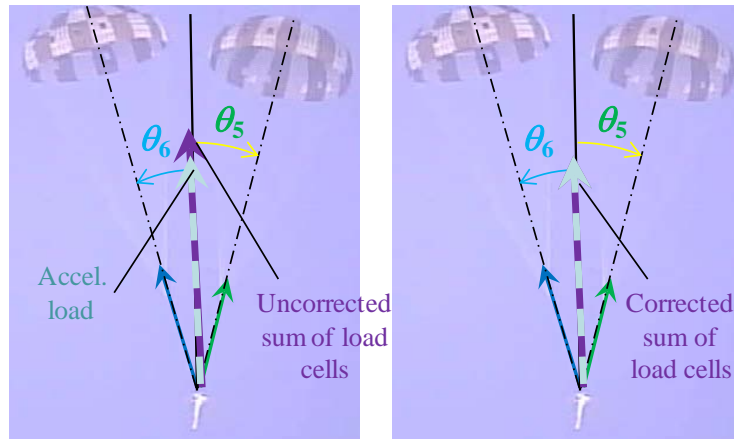


Figure 9. CDT-3-2 EDU Main parachute loads without (left) and with (right) correction for fly-out angles.

$$F = \sum_{i=1}^{i=N_c} (F_i \cdot \cos \theta_i) \quad (13)$$

As shown in Figure 10, the fly-out angle correction reduces the total scaled load cell data to better match the accelerometer-derived drag area.

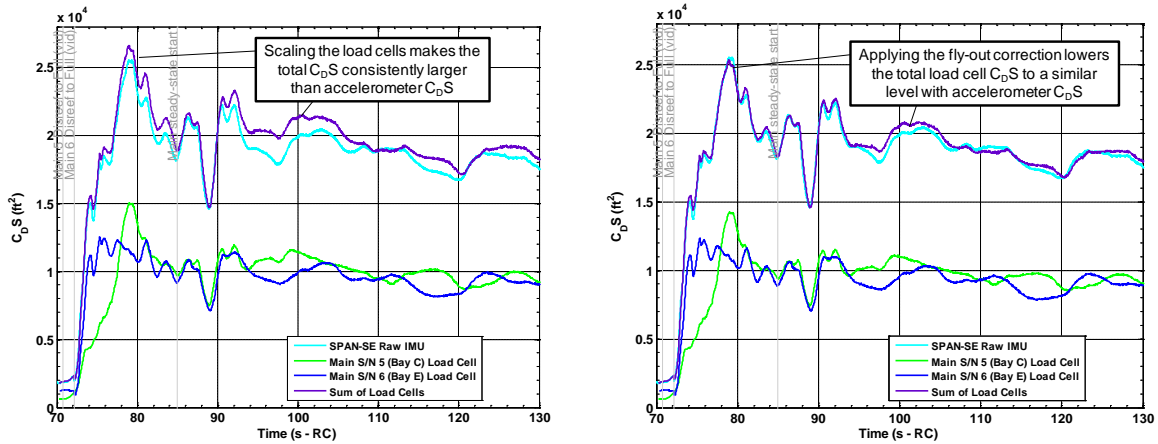


Figure 10. Main parachute drag area comparison without (left) and with (right) correction for fly-out angles.

IV. Overview of Inflation Reconstruction

Once the flight test data has been reduced, the inflation can be described by matching the drag area growth curves, $(C_D S)(t)$. The equation used to model drag area is described in detail in Ref 10. Simulations are therefore anchored to the test data by using inflation parameters which best fit the test data. The simulation tools and analysis methods have evolved over the course of the program.¹¹ Most notably, the simulations have recently transitioned from modeling a cluster as a single “composite parachute” towards modeling each parachute individually.

Where possible, the reduction of test data and matching the inflation profiles has been automated for speed and to reduce subjectivity. The current process is outlined in Figure 11. Vehicle mass properties and measurements of the vehicle initial state are used to create an input file for the Decelerator System Simulation (DSS)¹² or other simulation. Parameters from the current CPAS Model Memo¹³ are used as an initial guess of the inflation parameters for the test parachutes. Drag coefficient and reefing ratios are calculated from the flight data. All input parameters are checked by co-plotting the simulation outputs with the flight data. Parameters are then changed iteratively until a best fit is found. Until recently, this iteration was performed manually and the resulting inflation parameters were based on the judgment of the engineer performing the reconstruction. Once determined, these parameters and the models are collected into the next Model Memo.

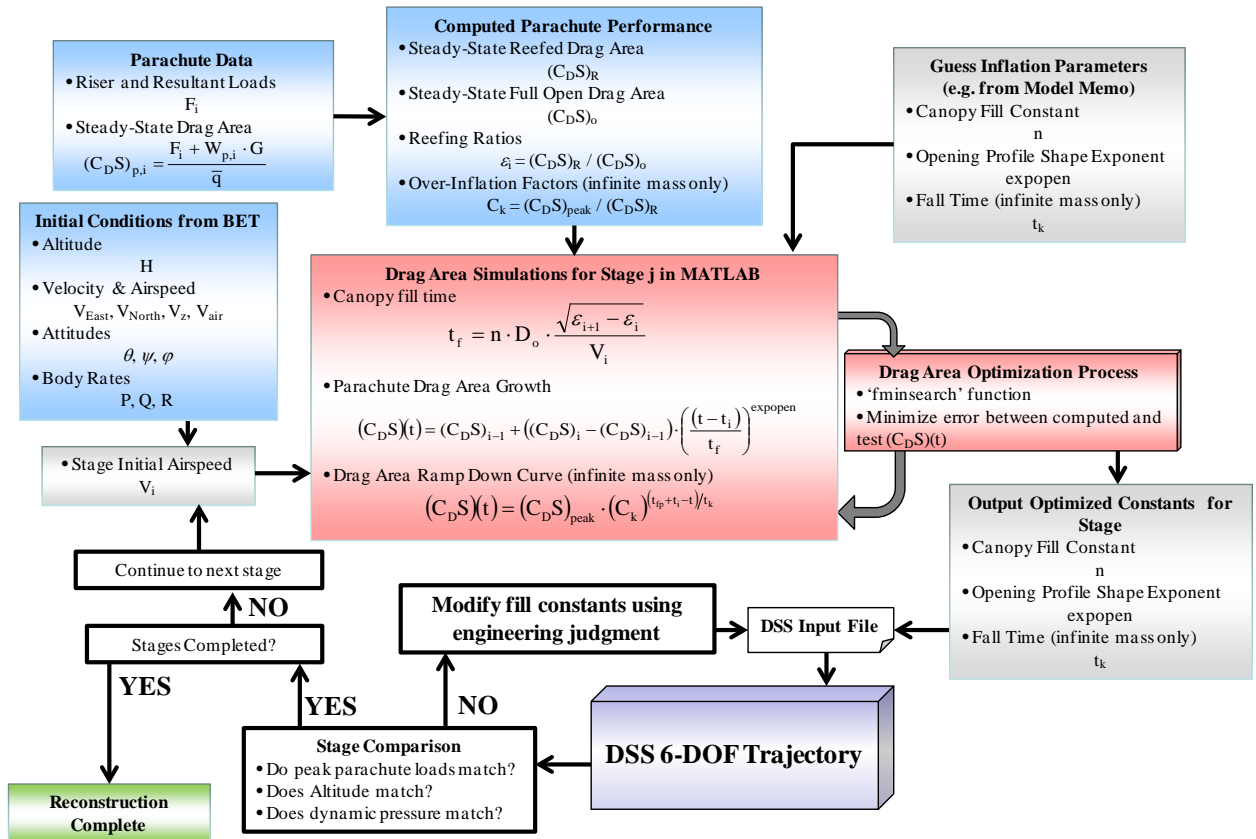


Figure 11. Parachute reconstruction process with automation.

V. Infinite Mass Inflations

The CPAS Forward Bay Cover Parachutes (FPCPs), Drogue parachutes, and Pilot parachutes are all considered to experience infinite mass inflations. That is, the inflation event is fast enough that no discernible deceleration occurs until after the inflation is complete. Infinite mass inflations are also characterized by an over-inflation where the canopy skirt initially becomes larger than its equilibrium size. To date, CPAS has only directly reconstructed the inflation of Drogue parachutes. The FBCP and Pilot parameters are currently assumed to have inflation parameters identical to those of the Drogue reconstructed first stage, but with smaller inflated drag areas.¹⁴

A. Drag Area Matching Process

The steps to match the drag area growth of typical infinite mass inflation are listed below and illustrated with an example in Figure 12. The “fminsearch” function in Matlab will iteratively adjust inputs to minimize an error function. In this case, the error function is the sum of the difference between each test data point and the theoretical curve, presented as a shaded area in the figure.

- Determine parachute parameters from test data:
 - Start time, t_i
 - Initial Airspeed, V_i
 - Time average drag areas
 1. Start Drag Area, $(C_D S)_{i-1}$
 2. End Drag Area, $(C_D S)_i$
 - Or equivalently describe reefing area ratios
 1. Drag coefficient, C_D
 2. Reefing Ratios, $\varepsilon_{i-1}, \varepsilon_i$
- Find the peak drag area point $[(C_D S)_{peak}, (t_{fp} + t_i)]$
 - Or specify point, if later data rises above inflation peak
 - This point defines $C_k = (C_D S)_{peak} / (C_D S)_i$

3. Generate inflation growth curve with guessed parameter:
 - Profile shape, expopen
 - Compute n as $f(\text{expopen})$
4. Compute difference between inflation curve and test data
5. Sum the difference to compute area between curves (error)
6. Iterate expopen to minimize the error area

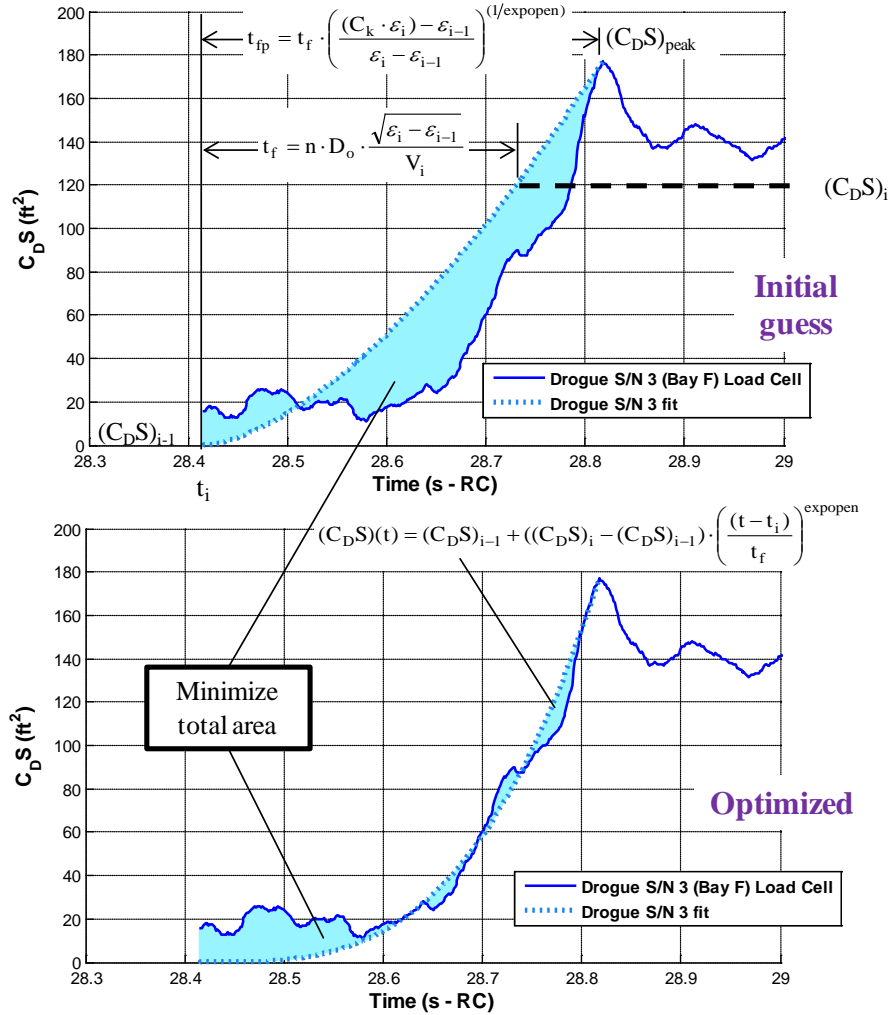


Figure 12. Infinite mass drag area growth curve fit example.

The decay time can also be optimized with a similar process shown in Figure 13. Because the test data has oscillations after the peak drag area, the automated values of t_k tend to be longer than from previous manual reconstructions. A larger value of t_k can lead to slightly higher peak loads (though this may be due to the current mortar deployment model), so the optimized method is generally more conservative.

1. Only examine data from $(C_D S)_{\text{peak}}$ to end of stage
2. Generate inflation decay curve with guessed parameter:
 - Decay time, t_k
3. Compute difference between decay curve and test data
4. Sum the difference to compute area between curves (error)
5. Iterate t_k to minimize the error area

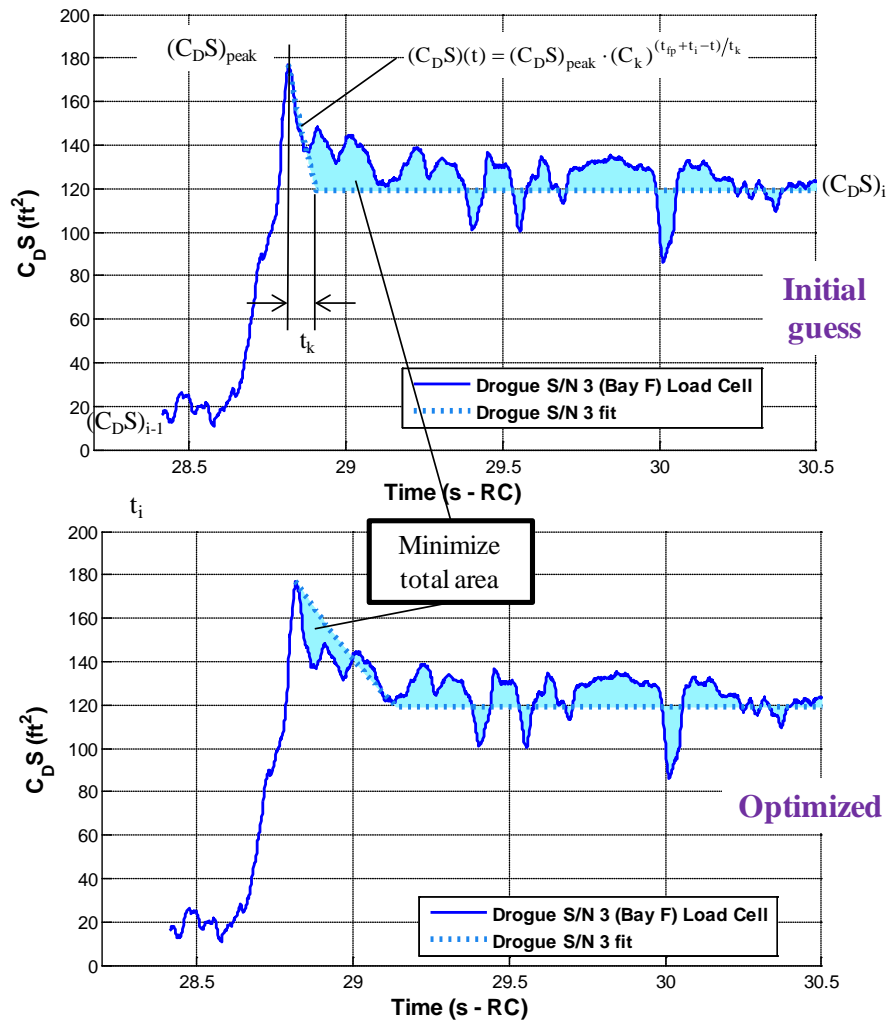


Figure 13. Infinite mass drag area decay curve fit example.

B. Drogue Deployment Inflation

Both CPAS EDU Drogues are independently mortar deployed and thus inflate at different times based on their deployment trajectories. An example of the typical variation is shown in the upward-looking high speed video in Figure 14 from CDT-3-2. The corresponding drag area traces (blue and red) shown in the figure demonstrate that the peak drag areas are not simultaneous. Had the inflations been simultaneous, the peak total drag area (purple) would have been significantly higher. Therefore, reconstructing Drogues individually better represents the underlying

physics of the situation. Further, inflation parameters reconstructed as a composite parachute may ultimately produce simulated loads which are overly conservative.

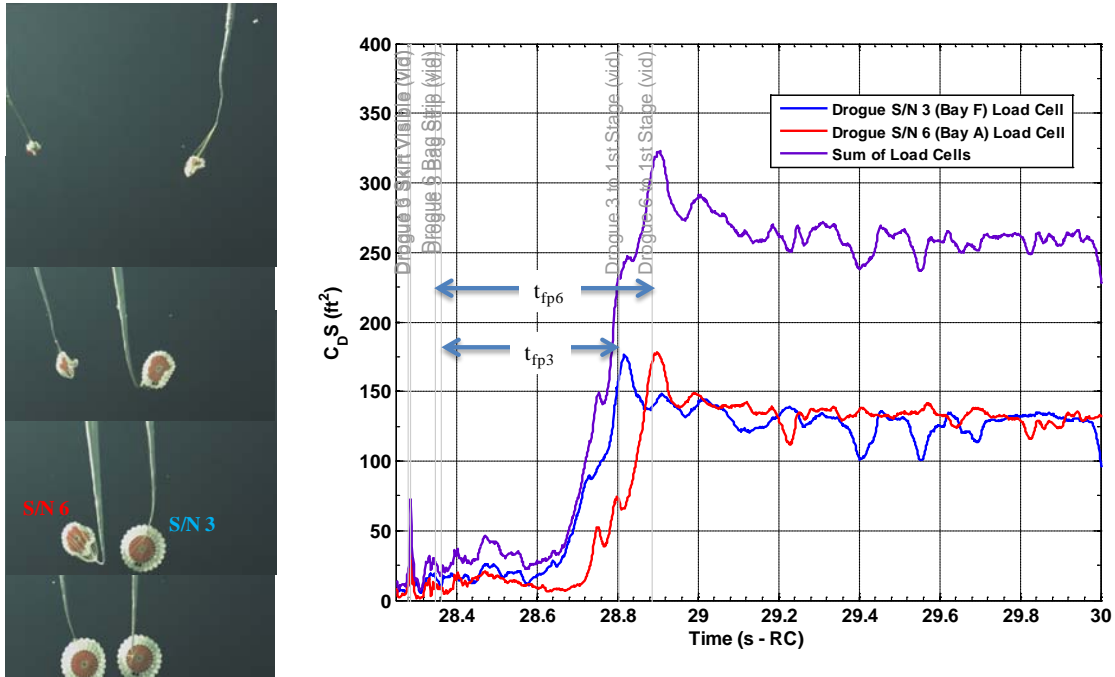


Figure 14. Typical non-simultaneous EDU Drogue inflation from high speed video (left) and drag area histories (right).

The optimized 1st stage drag area growth curves for each Drogue parachute are plotted as dotted lines in Figure 15. The sum of these drag areas is plotted as a grey dashed line. The optimized inflation parameters were then input into a DSS 6-DOF reconstruction. The output dynamic drag area is plotted as a black curve. Because the DSS includes a riser elastic spring model and added mass model, the resulting dynamic drag has more ringing than the total theoretical drag area growth curve.

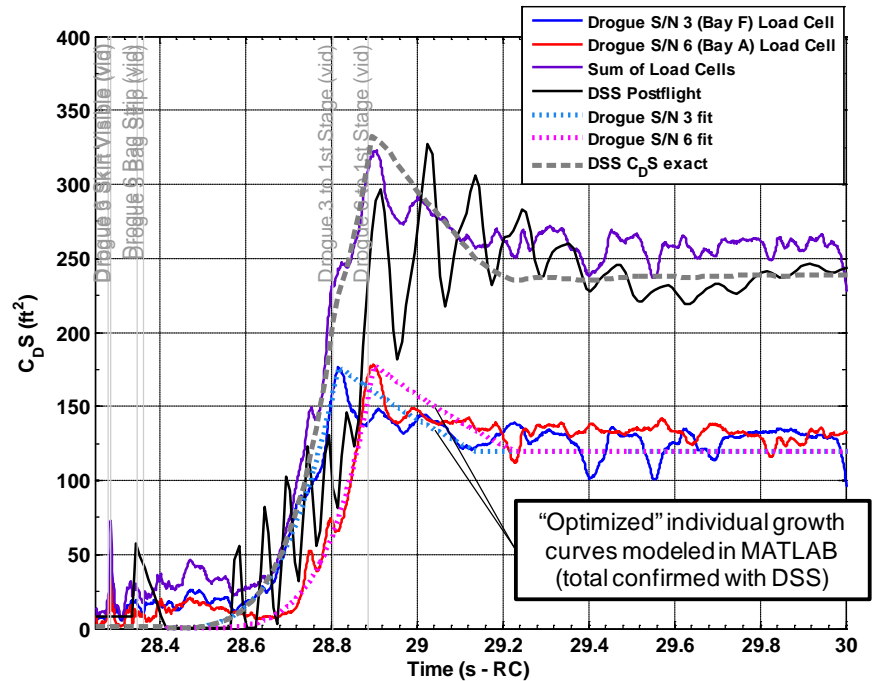


Figure 15. Reconstructed independent EDU Drogue drag area inflations.

As an alternative to the independent parachute reconstructions, a composite reconstruction of the total parachute drag area is presented in Figure 16. Because a composite reconstruction limits the inflation growth to a continuous curve, it does not match the compound curves produced by an independent parachute reconstruction.

The final check of the reconstruction is evaluating the total simulated loads. The resulting load compares favorably to the test data as shown in Figure 17.

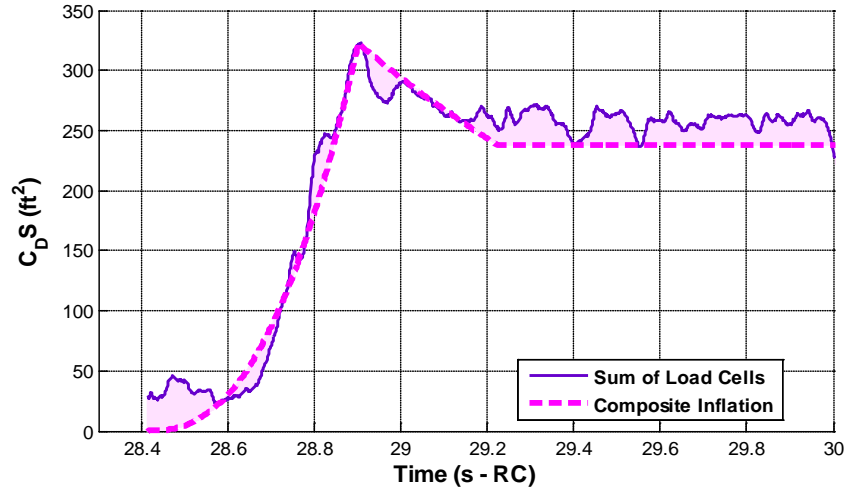


Figure 16. Reconstructed composite total Drogue drag area inflation.

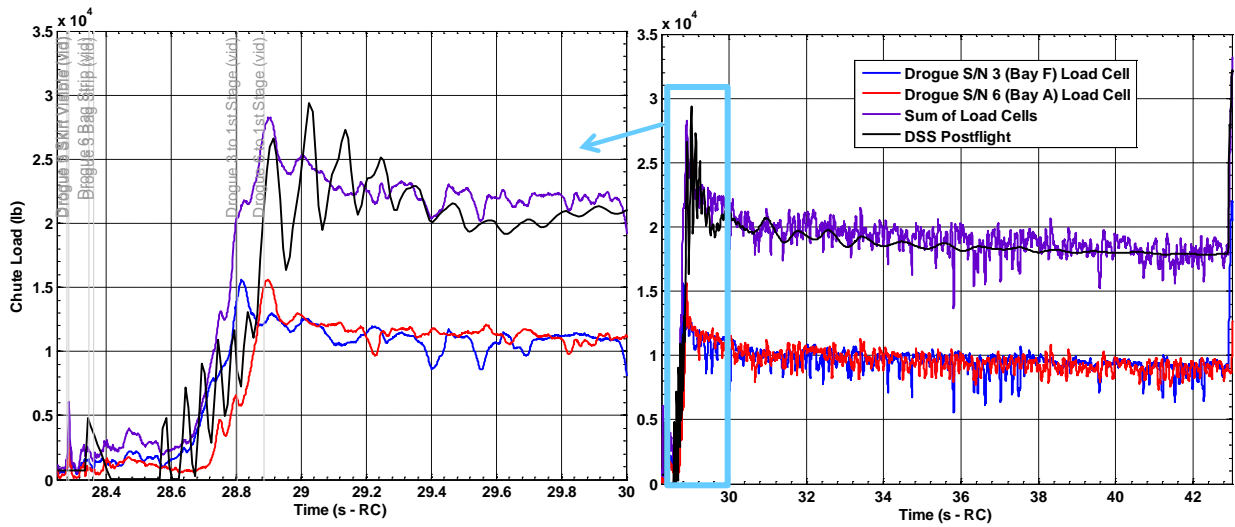


Figure 17. Reconstructed total Drogue inflation load.

C. Drogue Disreef Inflation

To manage peak inflation loads, the CPAS Drogue phase begins with two reefed stages before disreefing to full open. The variation in disreef cutter timing is usually on the order of a disreef fill time. For example, Figure 18 shows a typical case where one of the Drogues has completely disreefed before the other Drogue begins disreefing. This particular example from CDT-3-2 removed the second reefing stage altogether. Had both disreef cutters activated simultaneously, the total drag area and growth rate would be higher.

The individual loads traces were reconstructed using the Matlab optimization method and are shown as dotted lines with the test data.

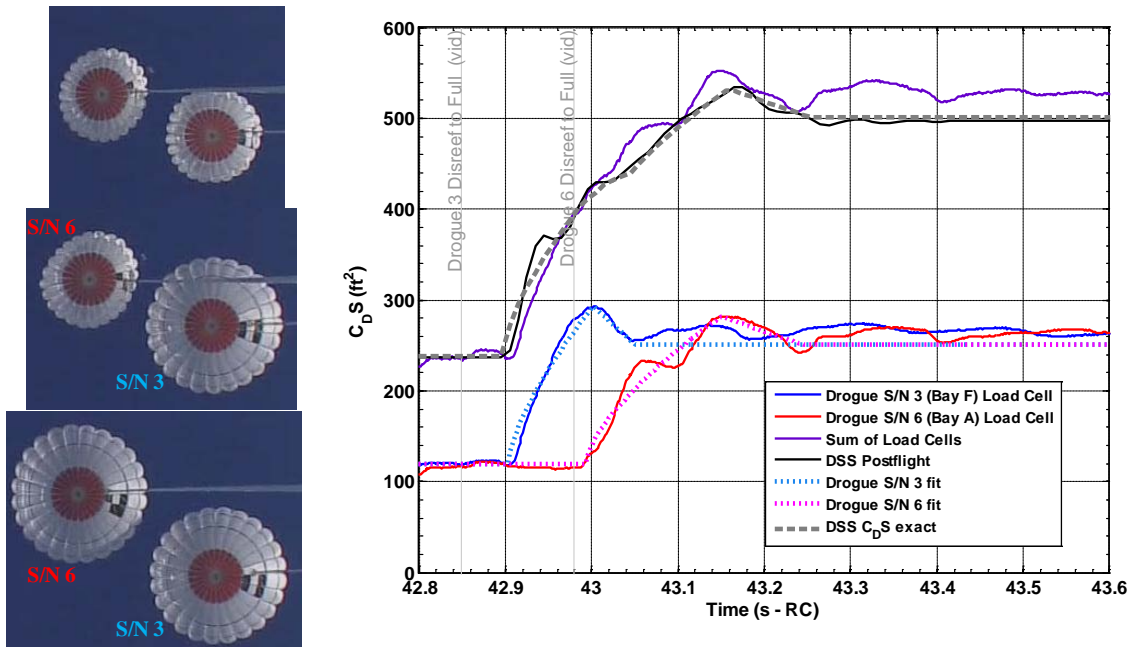


Figure 18. Typical non-simultaneous EDU Drogue disreef images (left) and drag area histories (right).

In contrast, a composite reconstruction of the total drag area is shown in Figure 19. By its nature, it will lack the compound curvature possible in the individual parachute reconstruction. Simulations using composite reconstruction data will not be able to disperse the staggered reefing cutter timing as an independent degree of freedom.

The simulated total cluster load is confirmed to match the test data in Figure 20.

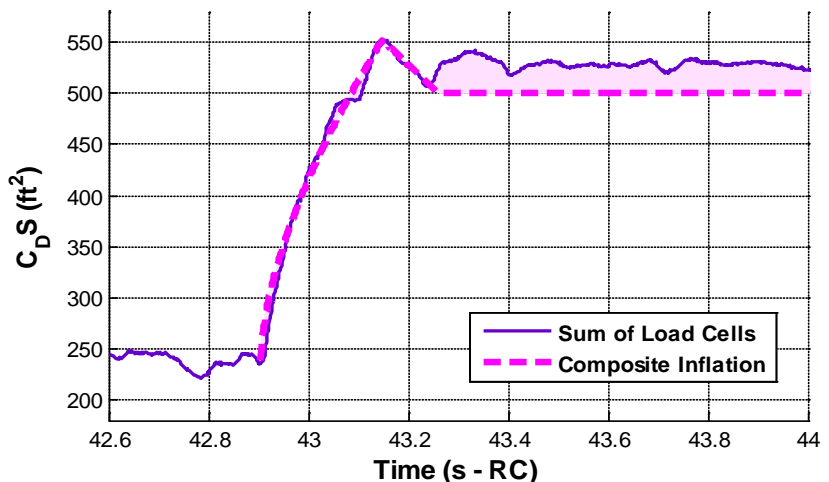


Figure 19. Reconstructed composite total Drogue disreef drag area.

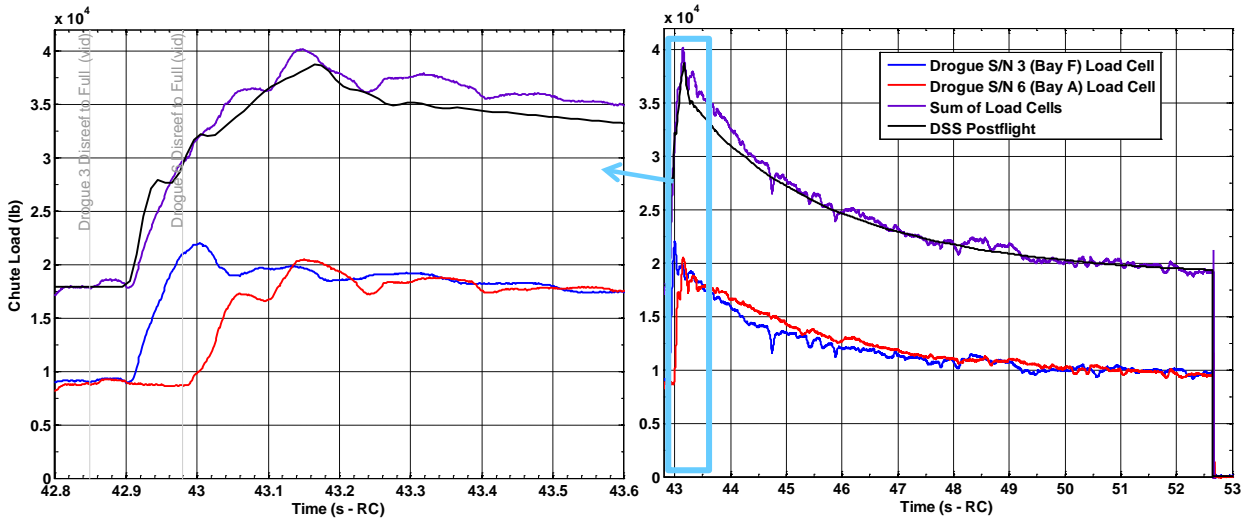


Figure 20. Reconstructed total Drogue disreef load.

D. Re-parameterization

As discussed in Ref. 10, the drag area growth curve parameters are not independent. For a given initial airspeed and reefed condition, a finite mass fill time is defined by the fill constant parameter, n . However, the time to the peak drag area will vary based on the other factors. The variation in peak fill time is affected by expopen in a non-linear manner, as shown in Figure 21, if other factors are held constant.

The expopen term and over-inflation term, C_k , interact to affect the peak fill time. For an expopen less than 1.0, increasing the C_k will greatly increase the peak fill time, as shown on the left of Figure 22. When expopen is greater than 1.0, that same variation in C_k has a much smaller effect on peak fill time, as seen on the plot on the right of Figure 22.

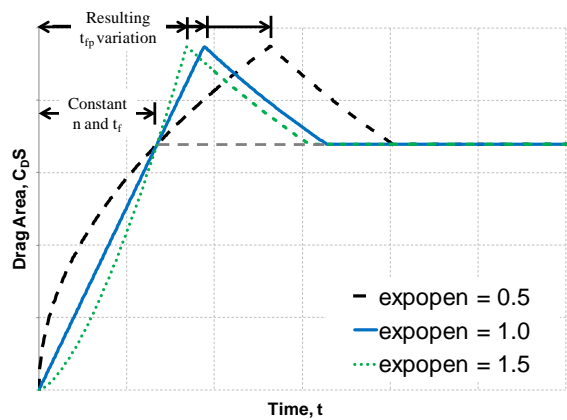


Figure 21. Peak fill time sensitivity to expopen.

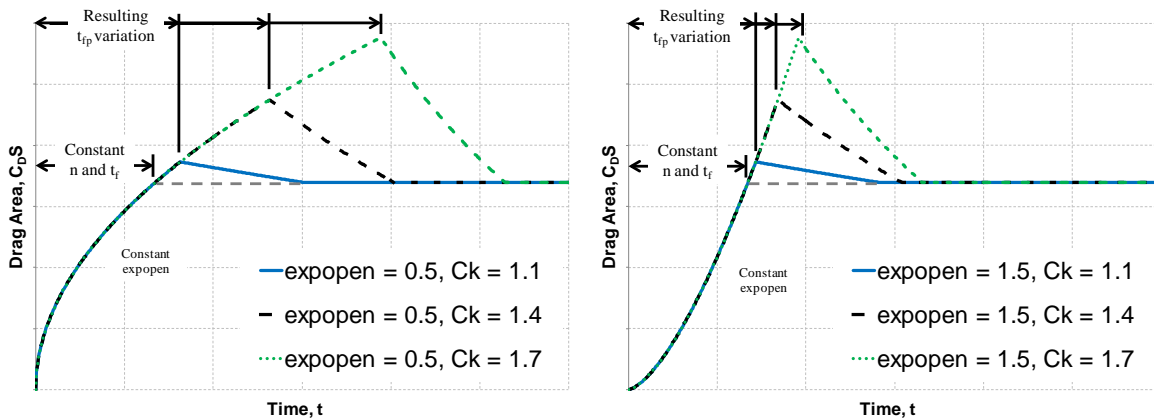


Figure 22. Peak fill time sensitivity to C_k for expopen less than 1.0 (left) and for expopen greater than 1.0 (right).

Thus it can be seen that in Monte Carlo simulations, varying the C_k and expopen parameters independently can result in unrealistic combinations of those parameters, resulting in long peak fill times that were never experienced in the flight tests from which the parameters were extracted. A way to avoid this situation is to re-parameterize the reconstructed data to describe the peak fill time directly.

This begins by considering the definition of fill time from Eq. 14 and the definition of peak fill time from Eq. 15. These are combined to describe peak fill time in terms of the fill constant, as in Eq. 16.

$$t_f = n \cdot D_o \cdot \frac{\sqrt{(C_D S)_i - (C_D S)_{i-1}}}{V_i} \quad (14)$$

$$t_{fp} = t_f \cdot \left(\frac{(C_k \cdot (C_D S)_i) - (C_D S)_{i-1}}{(C_D S)_i - (C_D S)_{i-1}} \right)^{(1/\text{expopen})} \quad (15)$$

$$t_{fp} = n \cdot \left(\frac{(C_k \cdot (C_D S)_i) - (C_D S)_{i-1}}{(C_D S)_i - (C_D S)_{i-1}} \right)^{(1/\text{expopen})} \cdot D_o \cdot \frac{\sqrt{(C_D S)_i - (C_D S)_{i-1}}}{V_i} \quad (16)$$

Next, n_p is defined such that it describes the time until the peak load. This expresses the peak fill time using the same parameters that originally normalized the fill time. The n_p parameter is defined in Eq. 17.

$$n_p = n \cdot \left(\frac{(C_k \cdot (C_D S)_i) - (C_D S)_{i-1}}{(C_D S)_i - (C_D S)_{i-1}} \right)^{(1/\text{expopen})} \quad (17)$$

To use this term, all the flight test data reconstructions convert n to n_p . A best-fit distribution of n_p is created for each stage. This ensures that no simulation will encounter an excessive peak fill time, because they will be explicitly limited to those times experienced by the tests.

The current 6-DOF simulations still require an n value for input. This is achieved by first dispersing n_p , C_k , expopen, and reefing ratios using the established dispersion rules. Then the corresponding fill constant for each run is computed using Eq. 18.

$$n = n_p \cdot \left(\frac{(C_k \cdot (C_D S)_i) - (C_D S)_{i-1}}{(C_D S)_i - (C_D S)_{i-1}} \right)^{(-1/\text{expopen})} \quad (18)$$

An example of a specified n_p is shown in Figure 23. The constant n_p will define a peak fill time regardless of the other inflation parameters. In the example, expopen is varied, which has the effect of changing the fill time. However, it is much more likely that the dispersed values of fill time are within the experience of flight test.

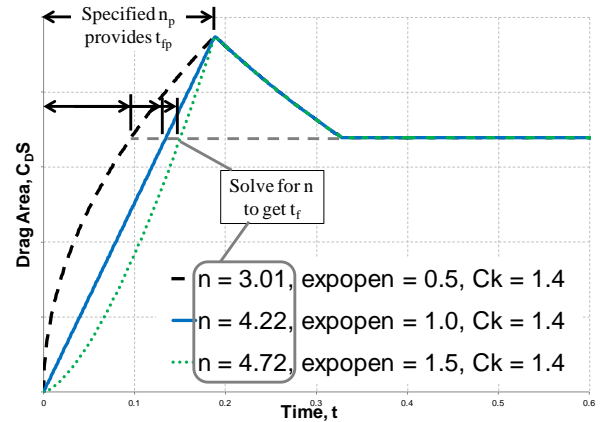


Figure 23. Fill time sensitivity to expopen for a specified peak fill time.

VI. Finite Mass Inflations

The CPAS Main parachutes experience a finite mass inflation. This means that the inflation process is relatively slow enough that the vehicle has significantly decelerated by the time the inflation stage is complete.

A. Drag Area Matching Process

The finite mass optimization steps are outlined below with an example illustrated in Figure 24. The time average of the ending drag area for first or second stage depends on the endpoints chosen. However, sometimes this is not clear, as often a Main parachute stage takes a large time to develop. Therefore, an additional optional step to best fit the final drag area reefing has been added.

By CPAS convention, full open performance for the Mains is defined by an equilibrium vertical velocity drag coefficient, C_{D_o} , which is based on rate of descent statistics.¹⁵ This is because the Mains have significant cluster dynamics during steady-state that cause variations in the vertical velocity.⁸

1. Determine parachute parameters from test data:
 - Start time, t_i
 - Initial Airspeed, V_i
 - Determine full open drag coefficient based on equilibrium vertical velocity, C_{D_o}
 - Time average drag areas for reefed stages, based on:
 1. Start Drag Area of the stage, $(C_D S)_{i-1}$
 2. End Drag Area of the stage, $(C_D S)_i$
 3. Full open drag area, $(C_D S)_o$
 - Or equivalently describe stages with area reefing ratios, ε_{i-1} , ε_i
2. Generate inflation curve with guessed parameters:
 - Fill constant, n
 - Profile shape, expopen
 - Optional: guess ε_i
3. Compute difference between inflation curve and test data
4. Sum the difference to compute area between curves (error)
5. Iterate n and expopen to minimize the error area
 - Optional: optimize ε_i

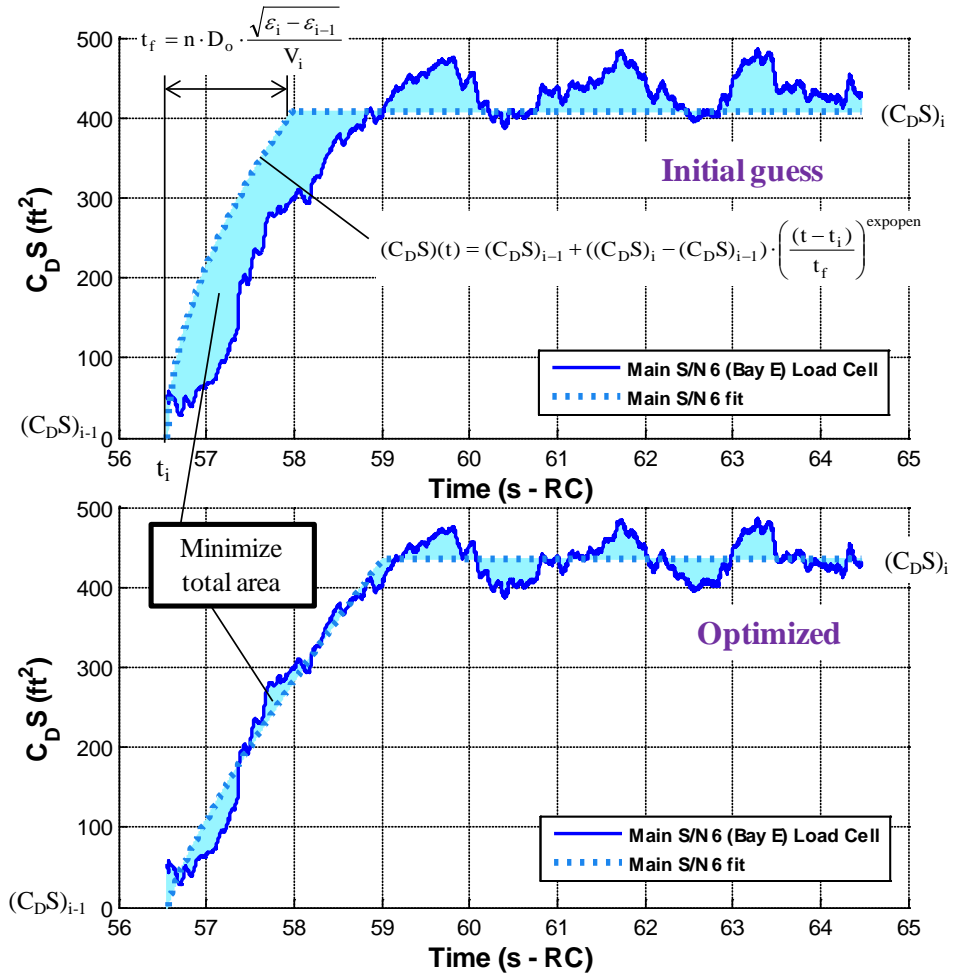


Figure 24. Finite mass drag area growth curve fit example.

B. Main Initial Inflation

The CPAS Mains are deployed by the CPAS Pilot parachutes. Because each mortar-deployed Pilot follows a unique path and then lifts its corresponding Main deployment bag individually, the Mains will all reach bag strip at slightly different times. DSS currently assumes all Mains begin inflating at the same time. An example of a three-Main cluster deployment is shown in Figure 25. Main S/N 3 is visibly the most inflated canopy in the cluster and has the highest drag area in the accompanying trace. The optimization routine converged with Main S/N 3 completing its inflation at about 86 seconds after Ramp Clear (RC). Had a user manually chosen an earlier time, then the average reefed drag area would be lower.

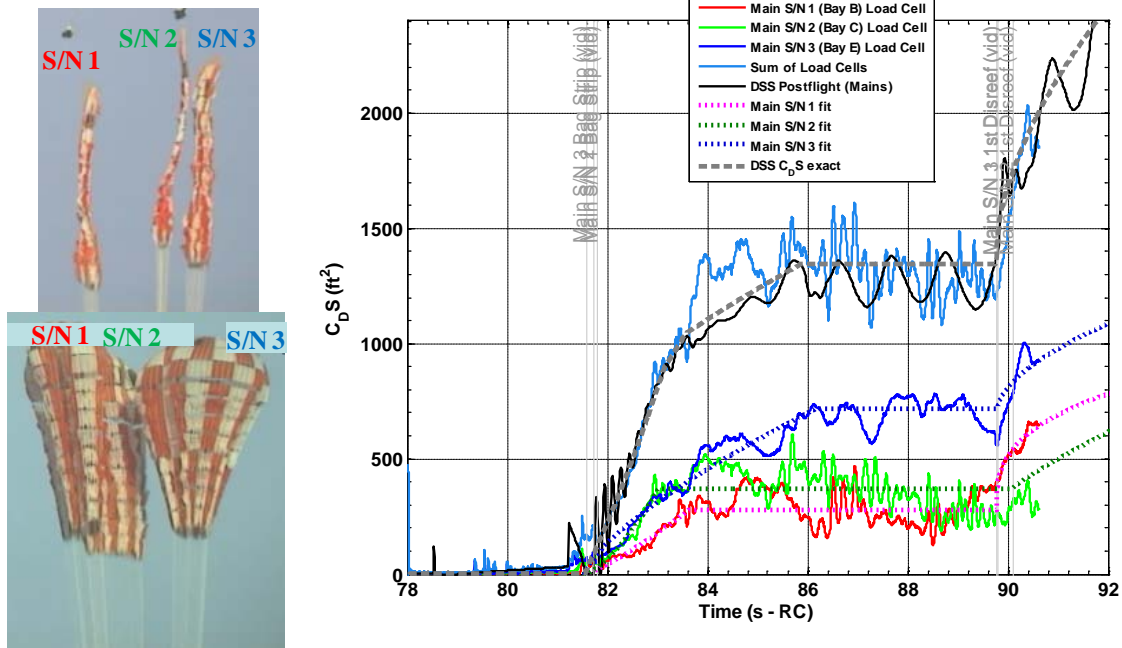


Figure 25. Sample reconstructed independent EDU Main 1st stage drag area inflations.

By optimizing the drag areas matching, the resulting total simulated peak load from DSS is close to the sum of the load cell data, as seen in Figure 26.

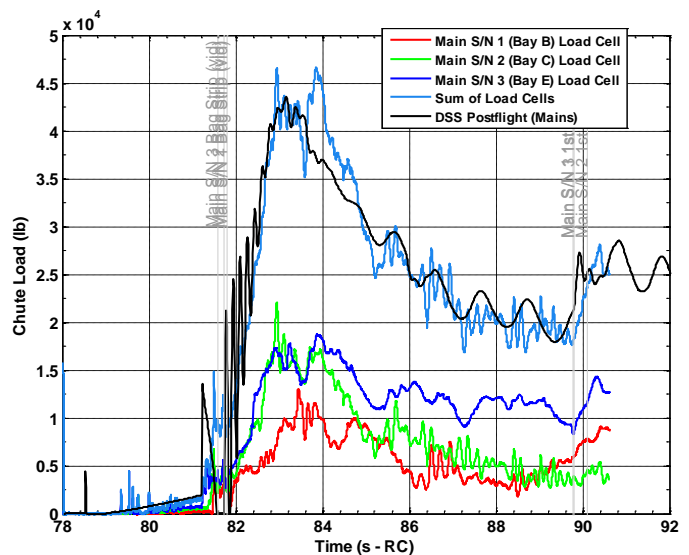


Figure 26. Sample reconstructed independent EDU Main 1st stage total load.

C. Main 1st Disreef Inflation

The normal staggering of disreef times are apparent from the video and CDT-3-3 test data in Figure 27. Again, Main S/N 3 is visibly largest and has the highest drag area. The Mains complete the second stage just about when the final disreef cutters fire.

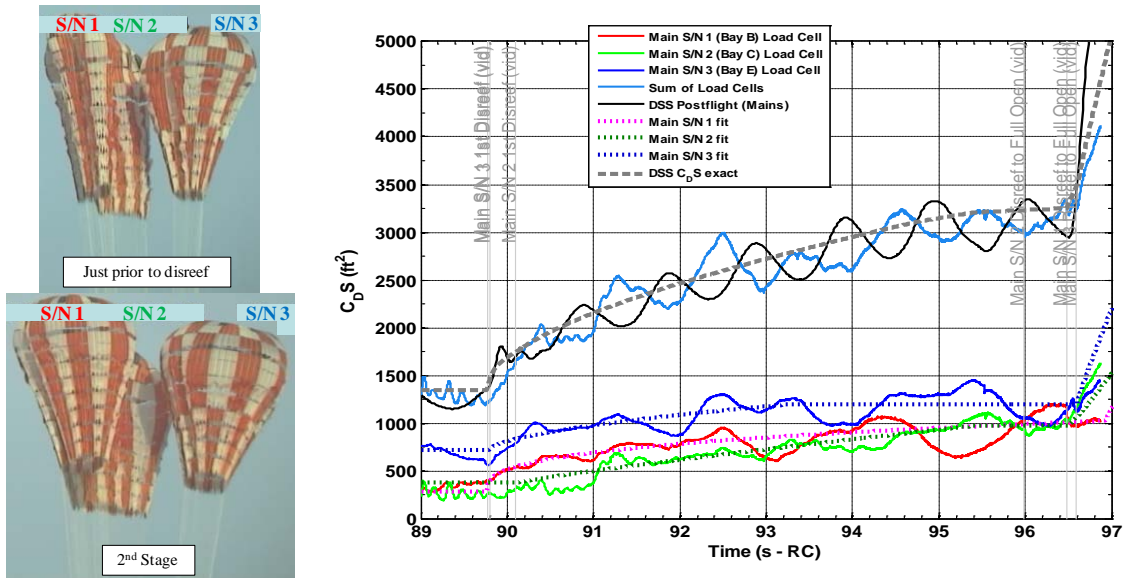


Figure 27. Sample reconstructed independent EDU Main 2nd stage drag area inflations.

The DSS peak cluster load has a similar magnitude to that of the sum of the test data, as seen in Figure 28. However, DSS tends to achieve this peak load earlier than the test data. This may be due to limitation in the added mass model.

Due to the long second stage fill times reconstructed from EDU tests (especially for skipped stage tests), it is quite possible that simulations will encounter cases where a stage has not fully inflated to the intended reefed drag area before the next disreef cutter fires. To avoid a sudden discontinuity in the simulation, the code should have the ability to retain the final drag area values at disreef. This is illustrated in Figure 29.

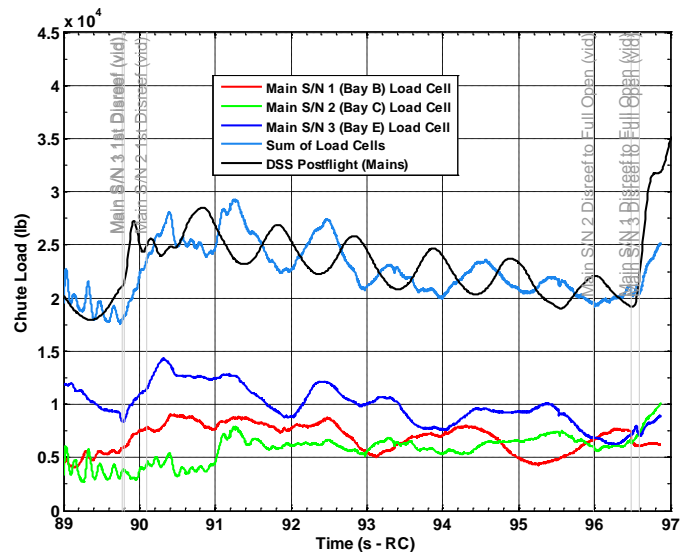


Figure 28. Sample reconstructed independent EDU Main 2nd stage total load.

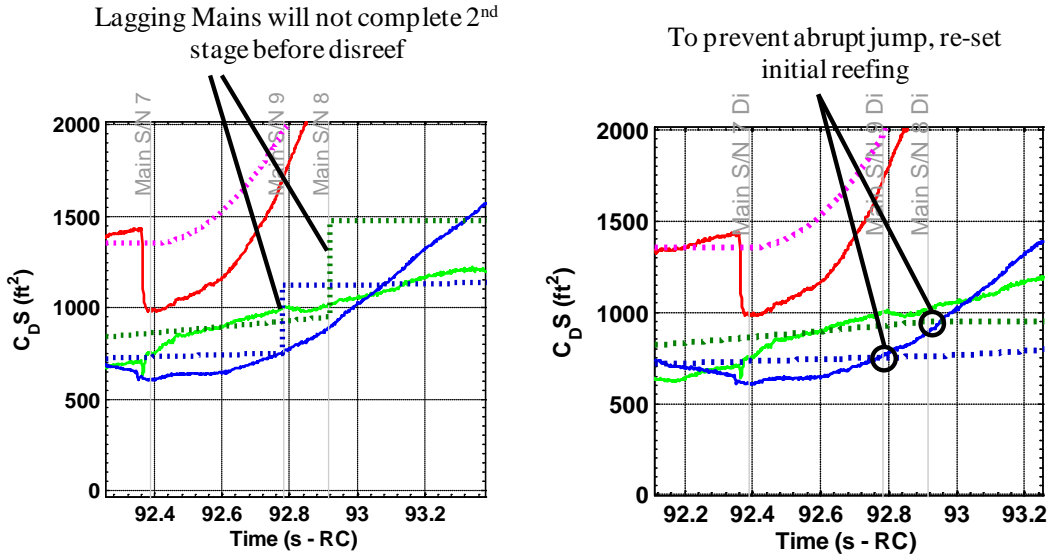


Figure 29. Sample simulation re-initialization of drag area to avoid reefing discontinuity.

D. Main Disreef to Full Open

The disreef to full open is shown in Figure 30. All three Mains are assumed to eventually grow to the same full open drag area based on the steady-state rate of descent. Future simulations will have the ability for each Main to inflate to slightly different full open drag areas. Because cluster dynamics are not currently modeled, the oscillations above the full open value do not occur in the individually reconstructed traces.

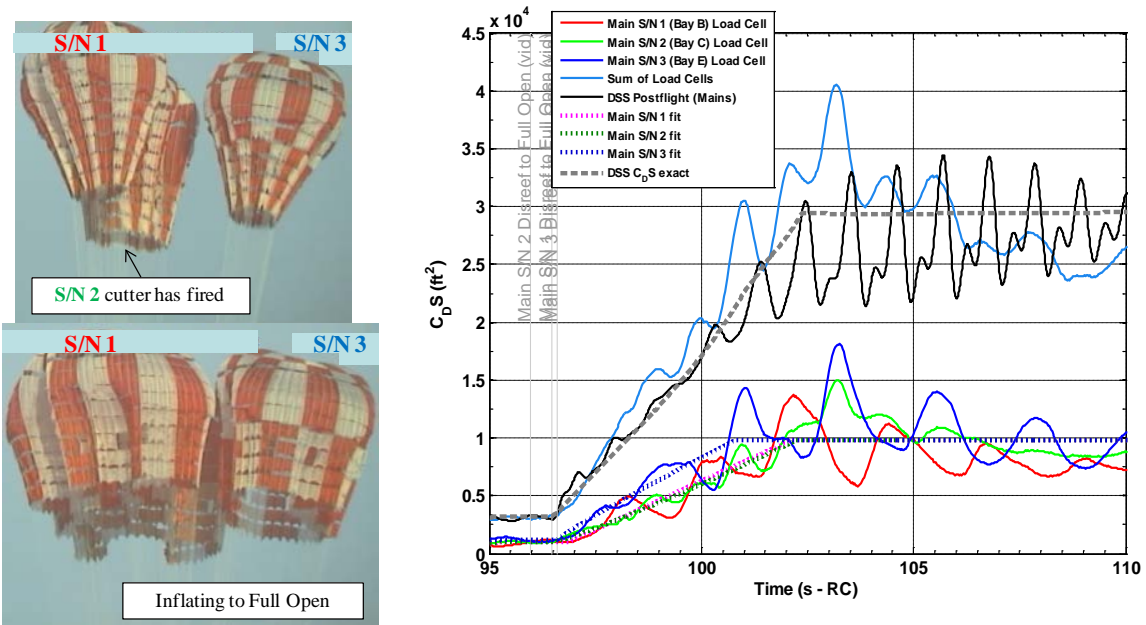


Figure 30. Sample reconstructed independent EDU Main full open inflation drag areas.

Nevertheless, the peak cluster load from DSS is a good match to the test data magnitude, as seen in Figure 31. As usual, the timing of the simulated peak load is slightly early.

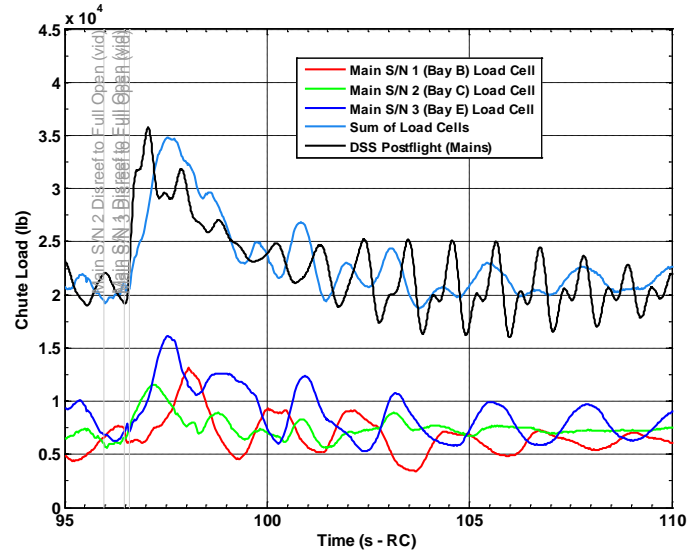


Figure 31. Sample reconstructed independent EDU Main full open loads.

VII. Conclusion

A method of reducing loads data from CPAS EDU parachute flight tests is presented. The equations used allow a direct comparison of test data with parameters from 6-DOF simulations of parachute inflations. CPAS is transitioning from simulating a cluster as a single parachute to modeling canopies individually, with the expectation that reduced conservatism in predicted loads will result. In order to measure individual EDU parachute loads, data from accelerometers and load cells are used to complement each other.

Once test data have been reduced, the inflations are reconstructed using the methods presented. The methods are tailored to infinite mass and finite mass inflations. This procedure has been applied independently to clusters of parachutes. Automation removes much of the subjectivity previously experienced with CPAS reconstructions. In the case of infinite mass inflations, the parameter used to describe the fill time has been replaced with a parameter to describe the time to peak drag area. This has the effect of de-coupling interactions that had previously caused some Monte Carlo simulations to result in unrealistic behavior.

Acknowledgments

The author wishes to acknowledge the contributions of Pete Cuthbert of NASA-JSC and James Dearman of Lockheed Martin in deriving the unsteady parachute equations.

References

- ¹ Moore, J. W., and Morris, A. L., "Development of Monte Carlo Capability for Orion Parachute Simulations," *21st AIAA Aerodynamics Decelerator Systems Technology Conference*, Dublin, Ireland, May 2011, AIAA paper 2011-2610.
- ² Ray, E. S., and Morris, A. L., "Challenges of CPAS Flight Testing," *21st AIAA Aerodynamics Decelerator Systems Technology Conference*, Dublin, Ireland, May 2011, AIAA paper 2011-2557.
- ³ Ray, E. S., and Morris, A. L., "Measurement of CPAS Main Parachute Rate of Descent," *21st AIAA Aerodynamics Decelerator Systems Technology Conference*, Dublin, Ireland, May 2011, AIAA paper 2011-2545.
- ⁴ Fraire, U., Dearman, J., and Morris, A. L., "Proposed Framework for Determining Added Mass of Orion Drogue Parachutes," *21st AIAA Aerodynamics Decelerator Systems Technology Conference*, Dublin, Ireland, May 2011, AIAA paper 2011-2546.
- ⁵ Wheeler, Anthony J. and Ganji, Ahmad R., *Introduction to Engineering Experimentation*, Prentice-Hall, Inc., 1996.

- ⁶ NovAtel, Inc., “IMU-HG,” NovAtel, Inc. web site [online], 2009, URL: http://www.novatel.com/assets/Documents/Papers/HG1700_SPAN58.pdf [cited 18 August 2010].
- ⁷ NovAtel, Inc., “SPAN-SE,” NovAtel, Inc. web site [online], February 2010, URL: <http://novatel.com/Documents/Papers/SPAN-SE.pdf> [cited 23 March 2010].
- ⁸ Ray, E. S., Bretz, D. R., and Morris, A. L., “Photogrammetric Analysis of CPAS Main Parachutes,” *21st AIAA Aerodynamics Decelerator Systems Technology Conference*, Dublin, Ireland, May 2011, AIAA paper 2011-2538.
- ⁹ Ray, E. S. and Bretz, D. R., “Improved CPAS Photogrammetric Capabilities for Engineering Development Unit (EDU) Testing,” *22nd AIAA Aerodynamic Decelerator Systems Technology Conference*, Daytona Beach, Florida, March 2013 (submitted for publication).
- ¹⁰ Schulte, P. Z., Moore, J. W., and Morris, A. L., “Verification and Validation of Requirements on the CEV Parachute Assembly System Using Design of Experiments,” *21st AIAA Aerodynamics Decelerator Systems Technology Conference*, Dublin, Ireland, May 2011, AIAA paper 2011-2558.
- ¹¹ Morris, A. L., *et al.*, “Simulating New Drop Test Vehicles and Test Techniques for the Orion CEV Parachute Assembly System,” *21st AIAA Aerodynamics Decelerator Systems Technology Conference*, Dublin, Ireland, May 2011, AIAA paper 2011-2616.
- ¹² Cuthbert, P., “Decelerator System Simulation (DSS) Version 312,” June 2010, NASA, Houston, TX.
- ¹³ Ray, E. S., *et al.*, *Capsule Parachute Assembly System (CPAS) Engineering Development Unit Operating Modeling Parameters Version 11*, JSC 65914 Rev F, ESCG-8400-CPAS-10-CPAS-MEMO-0069 Rev F, November 2012, Jacobs Sverdrup Engineering and Science Contract Group.
- ¹⁴ Ray, E. S., Hennings, E., and Bernatovich, M. A., “Testing Small CPAS Parachutes Using HIVAS,” *22nd AIAA Aerodynamic Decelerator Systems Technology Conference*, Daytona Beach, Florida, March 2013 (submitted for publication).
- ¹⁵ Ray, E. S., and Morris, A. L., “Measurement of CPAS Main Parachute Rate of Descent,” *21st AIAA Aerodynamics Decelerator Systems Technology Conference*, Dublin, Ireland, May 2011, AIAA paper 2011-2545.